How to cite: *Angew. Chem. Int. Ed.* **2022**, *61*, e202107554
International Edition: doi.org/10.1002/anie.202107554
German Edition: doi.org/10.1002/ange.202107554

Adsorption

Palladium/Ferrierite versus Palladium/SSZ-13 Passive NOx Adsorbers: Adsorbate-Controlled Location of Atomically Dispersed Palladium(II) in Ferrierite Determines High Activity and Stability**

Konstantin Khivantsev[+], Xinyi Wei[+],* Libor Kovarik, Nicholas R. Jaegers, Eric D. Walter, Pascaline Tran, Yong Wang, and János Szanyi**

Abstract: *Pd-loaded FER and SSZ-13 zeolites as low-temperature passive NOx adsorbers (PNA) are compared under practical conditions. Vehicle cold start exposes the material to CO under a range of concentrations, necessitating a systematic exploration of the effect of CO on the performance of isolated Pd ions in PNA. The NO release temperature of both adsorbers decreases gradually with an increase in CO concentration from a few hundred to a few thousand ppm. This beneficial effect results from local nano-"hot spot" formation during CO oxidation. Dissimilar to Pd/SSZ-13, increasing the CO concentration above ≈1000 ppm improves the NOx storage significantly for Pd/FER, which was attributed to the presence of Pd ions in FER sites that are shielded from NOx. CO mobilizes this Pd atom to the NOx accessible position where it becomes active for PNA. This behavior explains the very high resistance of Pd/FER to hydrothermal aging: Pd/FER materials survive hydrothermal aging at 800 °C in 10 % H_2O vapor for 16 hours with no deterioration in NOx uptake/release behavior. Thus, by allocating Pd ions to the specific microporous pockets in FER, we have produced (hydro)-thermally stable and active PNA materials.*

Introduction

Improving air quality is one of the grand challenges in our society.[1,2] Since exhaust from internal combustion engines produces the majority of toxic NOx emissions, there is a continuing need to improve their effectiveness. Most recently, the ammonia selective catalytic reduction (SCR) technology which was first discovered in the 1970s[3] for Cu/Y zeolites was proposed for Cu/SSZ-13[4] and later implemented by BASF on a large scale.[4,5] Such technology successfully removes NOx[4,5] at temperatures above 200 °C, relying on a sacrificial ammonia source (urea), with copper ions dispersed in small-pore SSZ-13 zeolite being the catalytically active species. However, at low temperatures (< 150 °C), during vehicle cold start for example, known catalysts are incapable of performing this challenging reaction effectively. Furthermore, ammonia cannot be delivered successfully to the catalyst at temperatures < 180 °C when urea is used as the source of ammonia. In order to address the low-temperature cold start problem, Pd/zeolite materials were introduced as passive NOx adsorbers (PNA).[6–22] Conceptually, NOx is adsorbed at low temperature and released at temperatures when Cu/SSZ-13 is active for SCR (200 °C and higher). As it was recently shown, the active sites in these Pd-containing materials are isolated Pd ions located in the micropores of various zeolites.[6–20] Structure-adsorption property relationships have been revealed for a range of Pd/zeolite materials (SSZ-13, BEA, MFI, MWW, SSZ-39) and guidelines for the preparation of high-loadings of atomically dispersed materials have been disclosed.[6–27] More recently, FER materials were used to support Pd and their PNA performance has been evaluated.[21,22] Despite this success, there remains a formidable challenge to produce materials that *1)* retain hydrothermal stability up to 800 °C; 800 °C hydrothermal aging is an expedited aging protocol to simulate end of useful life for a material (such a benchmark would circumvent potential degradation stimulated by diesel particulate filter (DPF) regeneration since maximum exhaust gas temperatures reach up to ≈700 °C during this process) *2)* perform well in the presence of elevated levels of CO during cold start from a few hundred to a few thousand ppm, and *3)* exhibit excellent performance during consecutive PNA cycles and be regenerable. Herein, we compare the performance and stability of Pd/FER and Pd/SSZ-13 and derive novel structure-adsorption property relationships for these materials.

Pd/FER contains a specific isolated Pd site in the FER micropore that is inaccessible to adsorbates such as NOx and water. This site is activated and moved into a more accessible position in the presence of higher CO concentrations (> 500 ppm) and produces an excellent PNA material with

[*] Dr. K. Khivantsev,[+] Dr. L. Kovarik, Dr. N. R. Jaegers, E. D. Walter, Dr. Y. Wang, Dr. J. Szanyi
Institute for Integrated Catalysis
Pacific Northwest National Laboratory
Richland, WA 99352 (USA)
E-mail: Konstantin.Khivantsev@pnnl.gov
Janos.Szanyi@pnnl.gov
Dr. X. Wei,[+] Dr. P. Tran
Environmental Catalysis Research Division, BASF
Iselin, NJ 08830 (USA)
E-mail: Xinyi.Wei@basf.com
Dr. Y. Wang
Voiland School of Chemical Engineering and Bioengineering
Washington State University
Pullman, WA 99164 (USA)
[+] These authors contributed equally to this work.

[**] A previous version of this manuscript has been deposited on a preprint server (https://doi.org/10.26434/chemrxiv.12385577).
Supporting information and the ORCID identification number(s) for the author(s) of this article can be found under: https://doi.org/10.1002/anie.202107554.

a capacity similar to the best SSZ-13 materials. Moreover, higher CO partial pressure leads to the release of NOx in close to the ideal temperature range of ≈200–300 °C (depending on the effectiveness of SCR catalyst and the gap between the PNA and SCR zones) as a result of local nano-"hot spots" formation due to CO oxidation.

Through a series of detailed adsorption-desorption experiments it is shown that the NOx release temperature coincides with the onset of CO oxidation. We show the excellent performance of these materials under practically relevant conditions. Moreover, due to the presence of a specific Pd site in the FER micropores resistant to water hydrolysis during hydrothermal aging at 800 °C (and even 850 °C) in 10 % $H_2O/O_2/N_2$ mix for 16 hours, no changes in the adsorption of NOx occur, a feature that has not been previously achieved with any PNA material.[6–19] Although previously Pd/SSZ-39[14] showed stability of NOx uptake after aging at 800 °C, the NOx release profile broadened and shifted to higher temperatures which was not desirable (at CO levels ≈250 ppm in ref. [14]).

Results and Discussion

We have previously described structure-PNA performance property relationships for Pd/SSZ-13 with Si/Al ≈6.[7,9] In the dry state this material contains predominantly super-electrophilic Pd^{+2} sites held electrostatically by 2 oxygens associated with framework Al atoms (see HAADF-STEM images and FTIR during CO adsorption in Figures S1,2). In the previous studies,[6–19] CO levels around ≈200–250 ppm were used during NOx adsorption tests. However, there is continuous interest to test the performance in the presence of higher CO levels that are most relevant during cold start. Figure 1 A shows the comparison of the PNA performance of a 1 wt % Pd/SSZ-13 (Si/Al ≈6) material with ≈200 and 4000 ppm CO at a GHSV ≈150 L g^{-1} hr. We observe that increase in CO level does not change the NOx uptake. In contrast, the NOx release temperature changes significantly to lower temperature in the presence of higher concentrations of CO. This seems to coincide with the onset of CO oxidation activity. Since CO oxidation is highly exothermic, such CO concentrations create localized nano-hotspots that drive NOx off at lower temperatures (detailed *below* during discussion regarding Pd/FER). Ideally, all NOx would be released at temperature below ≈400 °C. Figure 1 B shows consecutive NOx uptake/release cycles on this material with varying levels of CO in the gas stream: the performance of Pd/SSZ-13 remains stable as long as all NOx is driven off from the material during temperature elevation. During the 12 consecutive cycles at CO concentration of either ≈200 or 4000 ppm, the NOx uptake and release remained nearly constant (the total amount of it; however, the temperature of release is significantly affected by the CO concentration (see our further discussion in the text), irrespective of the CO level. *In situ* EPR studies of Pd^{II}/SSZ-13 under relevant flow conditions in the presence of 1000 ppm CO demonstrated the absence of reduction of Pd^{II} to Pd^{I} or significant amounts of Pd^{0} (Figure S3), confirming the high stability of Pd^{II}/ 2Al sites in SSZ-13.

Pd/FER has received much less attention in the literature than other zeolites such as SSZ-13, BEA,[6–14] and more recently SSZ-39, MFI and MWW.[11,14] Lietti and co-workers very recently described the first example of utilizing Pd/FER system for NOx adsorption.[21] We utilize this system with Pd supported on H-FER with Si/Al ratio ≈10 and with a Pd loading of ≈1.8 wt %.[7,9] HAADF-STEM images for 1.8 % Pd/H-FER show highly crystalline FER material with Pd dispersed inside the pores as well as some ultra-small PdO clusters (<1 nm) decorating the periphery of the crystals (Figure 2 A,B, Figure S4, consistent with FTIR data during CO adsorption showing a minor fraction of CO adsorbed on metallic Pd clusters below <2090 cm^{-1} in Figure 2 C)), similar to that observed for Pd/SSZ-13 with Si/Al ratio ≈10–12

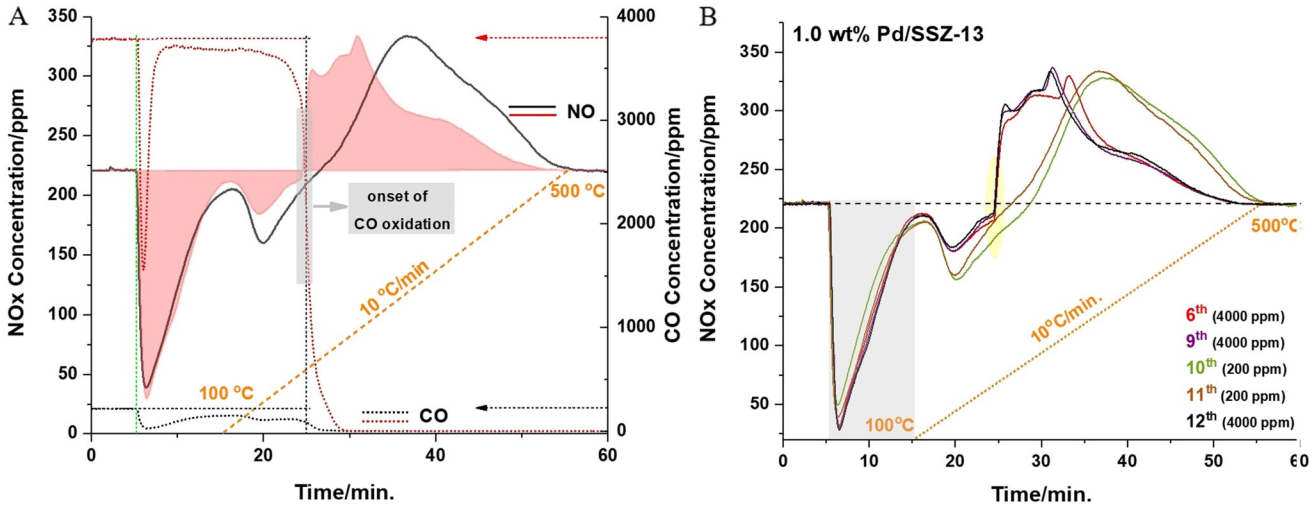

Figure 1. A. NOx (solid line) and CO concentration (dashed line) profiles for a 1 wt% Pd/SSZ-13 (Si/Al≈6) PNA in the presence of 200 ppm (black) and 4000 ppm CO (red). The orange line represents the temperature profile. [NOx uptake: at 100 °C for 10 min in 220 ppm NOx (200 ppm NO and 20 ppm NO_2), 200/4000 ppm CO, 14% O_2, 3% H_2O, balanced with N_2 at a flow rate of 300 sccm.] B. Comparison of PNA performance of the same material during repeated cycles with varying levels (200 and ≈4000 ppm) of CO in the feed.

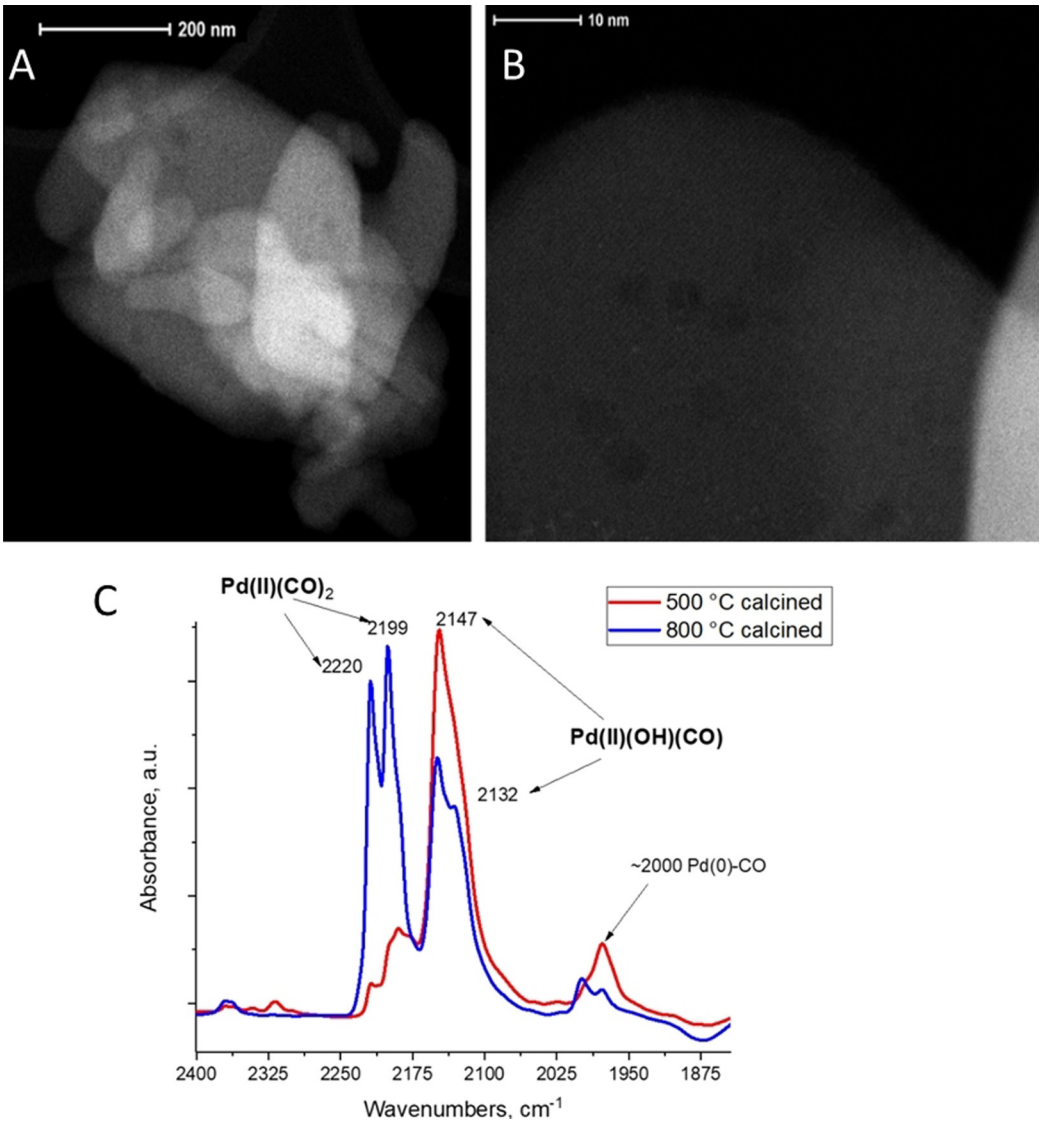

Figure 2. A. Low-magnification HAADF-STEM image of 1.8 wt% Pd/FER showing FER crystals with no sizable PdO nanoparticles observed. B. High-magnification HAADF-STEM image of 1.8 Pd/FER showing crystalline fringes of FER zeolite and absence of visible large PdO nanoparticles in the bulk or on the exterior. Other representative HAADF-STEM images of this sample are depicted in Figure S4. C. FTIR data during CO adsorption (10 Torrs) on in situ calcined (in air in the IR cell) at 500 °C (red spectrum) and 800 °C (blue spectrum) 1.8 wt% Pd/FER sample.

[Figure S5]. We chose to calcine the sample at 800 °C in oxygen because this treatment apparently produces the most active materials (Figure S6).

In situ infrared spectra employing CO probe molecules were collected to characterize the adsorption sites present in the fresh (pre-calcined in O_2 in the FTIR cell) and 800 °C-calcined (in the presence of oxygen) materials (Figure 2C). Substantial changes in the distribution of Pd species were observed as a result of calcination. Specifically, the IR spectrum of the freshly-calcined sample contains bands corresponding to mainly CO adsorbed on $[Pd^{II}(OH)]^+$ (at 2147–2132 cm^{-1}) complexes.[9] After 800 °C in situ calcination in air all the spectral features belonging to CO adsorbed undergo substantial changes (re-distribution). The intensities of the Pd(OH)-bound CO features decreased while the bands at 2220 and 2199 cm^{-1}, corresponding to CO adsorbed on Pd^{+2}/2Al ions[7,9] increased at their expense. These vibrational features are very similar to those we studied in details on Pd/SSZ-13, and assigned them to a $Pd^{II}(CO)_2$ complex formed on super electrophilic Pd^{II} ions in the zeolite. These results indicate that Pd cations can diffuse and re-distribute in the micropores of the FER framework during calcination at 800 °C, producing more active sites for NO adsorption (Figure S6). Cation diffusion was previously observed during in situ Rietveld refinement studies[29] for divalent metal cations in FER zeolite. More specifically, it was suggested that 3 specific sites can accommodate divalent (e.g., Ni, Mg, Co) cations: the α-site is located at the center of the 6-ring separating two ferrierite cages, the β-site is coordinated to the walls of the 10-MR channels while the γ-site is located inside the ferrierite cage, in a boat-shaped position.[30] The γ-site is the most sterically crowded site in FER. Clearly, the most

accessible sites are filled by Pd^{II} ions first, and their IR signatures correspond predominantly to $Pd^{II}(OH)(CO)$ species held by 1 Al atom (in such positions that are filled by Pd-OH first, obviously, no sites with 2 Al atoms in close proximity are available, otherwise a Pd^{II}/2Al site would form instead of Pd^{II}-OH because Pd^{II}/2Al is more thermodynamically stable than $Pd^{II}(OH)$/1Al site[7,9]). Upon heating, Pd cations diffuse and start to occupy less accessible positions, which, however, offer a different Al distribution that allows Pd^{II} to form thermodynamically preferred Pd^{II}/2Al sites. These FTIR findings provide the clear spectroscopic evidence of Pd^{II} ions movement and re-distribution in FER upon heating at 800 °C, showing a direct evidence of the processes previously suggested on the basis of Rietveld refinement studies. These data also suggest that Al distribution within different sites in FER is not uniform.

We would like to note that as of today, there existed no method to estimate the relative amounts of divalent metals in zeolites associated with either paired or unpaired Al sites. For some metals, such as cobalt it is accepted that basically no Co^{II}-OH sites form and cobalt exchanges as Co^{II}/2Al sites. However, for the majority of divalent metals, such as Pd^{II} and Cu^{II}, for example, both Pd(Cu)(II)-OH (associated with non-paired Al site) and Pd(Cu)(II) (associated with paired Al sites) can form. We have shown that it is possible to distinguish between them spectroscopically:[7,9] Pd^{II}-OH/1Al sites adsorb CO with the formation of a $Pd^{II}(OH)(CO)$ complex with CO vibrations in the ≈2140–2120 cm^{-1} range, whereas Pd^{II}/2Al sites adsorb CO with the formation of $Pd^{II}(CO)_2$ complex with CO frequencies for symmetric and asymmetric CO stretches of $Pd^{II}(CO)_2$ located at very high wavenumbers ≈2215 and ≈2195 cm^{-1} with a characteristic split of ≈20–21 cm^{-1}. This provides a way to not only spectroscopically probe Pd sites but also estimate the distribution of 1Al (singular) and 2Al (paired) sites available to a divalent metal. We believe this finding may have broad implications for the zeolite community to test divalent metal distribution and relative ratios between 1Al and 2Al sites accessible to these divalent metals.

Furthermore, we performed typical base (CD_3CN) adsorption of Pd/H-FER sample and H-FER (Figures S7–S9). The acidity differences are not significant because Pd loading is insignificant compared with total Al (and thus Bronsted acidity) sites (Figure S9). However, we utilized acetonitrile probe in a non-typical way by first adsorbing CO on Pd/FER samples having both Pd^{II}-OH and Pd^{II} cations: this produced $Pd^{II}(OH)(CO)$ and $Pd^{II}(CO)_2$ complexes (Figure S10). After evacuating excess CO, we chose to adsorb CD_3CN on the $Pd^{II}(OH)(CO)$ and $Pd^{II}(CO)_2$ complexes. Because acetonitrile is a cationic/metal "poison" and adsorbs very strongly on cationic and non-cationic metal sites, we observed its interaction with both $Pd^{II}(OH)(CO)$ and $Pd^{II}(CO)_2$ sites. This interaction becomes obvious because CD_3CN displaces the CO ligand by coordinating to $Pd^{II}(OH)$ and Pd^{II} sites. Interestingly, we found that $Pd^{II}(OH)(CO)$ complexes are more significantly affected by CD_3CN than $Pd^{II}(CO)_2$ complexes (which, as we suggested, form in more confined zeolitic positions) (Figure S10).

Based on the NOx/Pd ratio during PNA studies of these materials the majority (90%) of Pd is atomically dispersed and the NOx/Pd ratio is >0.9 for 4000 ppm CO in the feed. Figure 3A shows the performance of this material in the presence of ≈200 and 4000 ppm CO. A very significant shift of the NOx release is observed to lower temperatures with a sharp release of NOx at ≈200 °C and slightly broader feature at ≈250 °C. Figure 3B depicts NOx and CO profiles simultaneously during a NOx uptake/release cycle in the presence of 4000 ppm CO. At 200 ppm NOx concentration at the inlet, the NO release is completed at ≈350 °C with a maximum around 300 °C, which is more attractive than Pd/SSZ-13. In the presence of 4000 ppm CO the absorbed amount of NOx increases significantly (≈2 times) in com-

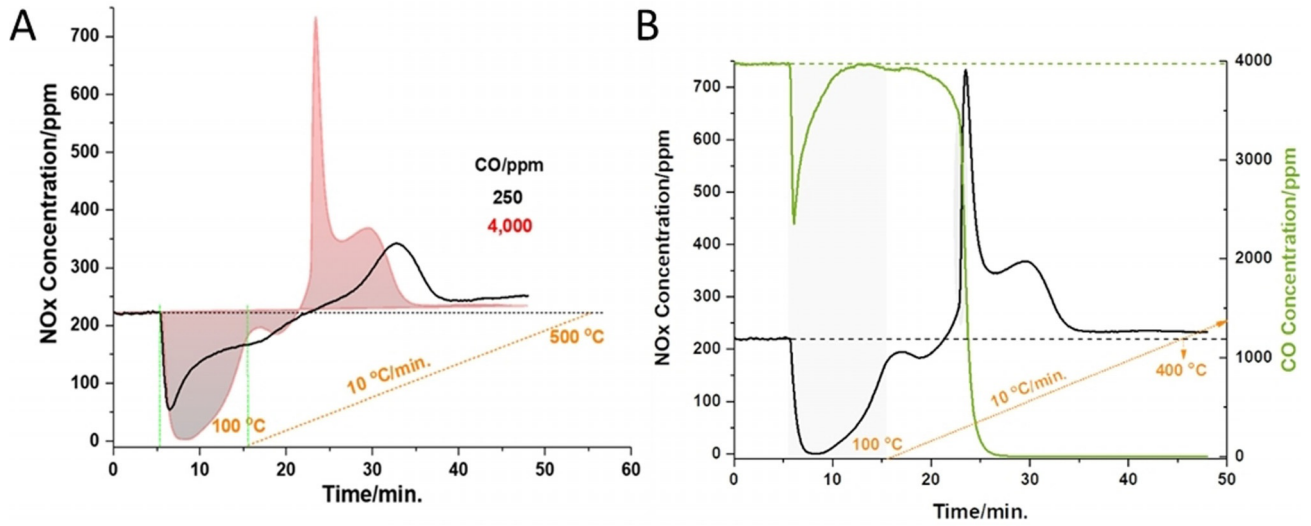

Figure 3. A. PNA performance of 1.8 wt% Pd/FER (Si/Al ≈10) (sample was hydrothermally aged at 800 °C). [220 ppm NOx (200 ppm NO and 20 ppm NO_2), 200/4000 ppm CO, 14% O_2, 3% H_2O, balanced with N_2 at a flow rate of 300 sccm.] NOx uptakes for the 250 ppm and 4000 ppm CO experiments were ≈0.45 and ≈0.9 NOx/Pd, respectively. B. Simultaneous CO and NOx profiles during PNA in the presence of ≈4000 ppm CO.

parison to that in the presence of 200 ppm CO. This behavior is completely different from that observed for Pd/SSZ-13 where the NOx uptake was not affected by the CO concentration in the gas stream (Figure 1). Moreover, additional tests with model Pd/FER (Figs. S11–S13) have shown that even ≈1000 ppm CO was sufficient to maximize NOx adsorption capacity. This is advantageous since cold-start (≈100 °C) exposes the material to high concentrations of CO. We have previously observed the formation of a mixed carbonyl nitrosyl complex [Pd^{II}(CO)(NO)] in Pd/SSZ-13 and it was confirmed that the formation of this mixed-ligand complex was responsible for the promoting mechanism CO has on NOx uptake in Pd/SSZ-13 and other Pd-containing materials.[7–10,13,23] Increasing CO levels higher than 200 ppm in the case of Pd/SSZ-13 (Si/Al = 6) does not increase NOx uptake since maximum adsorption capacity was already achieved with NO/Pd ratio near unity at Pd loadings up to 1.9 wt %. However, the phenomenon observed for Pd/FER is notably different. Two possible explanations for the significant promotion of NOx uptake by elevated CO levels (> 1000 ppm) are presented next.

First, the redispersion of small PdO particles and the formation of Pd^{II}(NO)(CO) mixed-ligand complex may be easier in the presence of high CO concentrations in the CO + NO mixture. However, the amount of Pd present as small clusters outside the zeolite should be much larger if this were the case. Moreover, when the sample is exposed to a CO + NO + O_2 + H_2O + N_2 mixture at 100 °C, we do not observe significant redispersion of these small PdO clusters based on microscopy (Figure S14); moreover, such clusters are not present in significant amounts. Alternatively, some isolated Pd^{II} ions located inside the micropores of FER are inaccessible for NOx adsorption. However, an adsorbate (CO), due to its strong interaction with Pd^{II}, is able to move those Pd ions to a more accessible location from their confined position where they become available for NOx adsorption. This peculiar behavior highlights a potential mechanism to control the location of a charge compensating cation by one adsorbate in order to enhance the adsorption of another adsorbate. Such a notable attribute has an application for synthesizing practically relevant materials which often need to sustain harsh hydrothermal aging at 800 °C in 10 % H_2O/air mixture for extended period. In the engine, during diesel particular filer (DPF) regeneration and overload the exhaust gas stream reaches temperatures sometimes up to 800 °C. Thus, practically viable materials must survive hydrothermal aging without much deterioration of adsorption capacity and similar (or better) adsorption-desorption behavior as the materials before aging. It was previously shown that the best Pd/SSZ-13 materials[12] lose ≈10–15 % of atomically dispersed Pd after HTA at 750 °C in 10 % H_2O/air mix for 16 hours. Pd^{II} ions are removed from their cationic positions by water hydrolysis (as hydrated mobile $Pd^{II}(OH)_2$ species) and then agglomerate into large PdO nanoparticles on the external SSZ-13 surface which are not easily redispersed by either oxidative heat or NO/O_2 treatment due to their large size.[12] Pd supported on large defect-free H-BEA crystals has shown high resistance to agglomeration at 750 °C in 10 % H_2O/air.[8] More recently, Pd/SSZ-39 was utilized for PNA and even though H-SSZ-39 crystals survived hydrothermal aging up to 1000 °C in 10 % H_2O vapor, Pd/SSZ-39 started to show signs of NOx uptake deterioration after HTA above 815 °C.[14]

Furthermore, after HTA the NOx release profile broadened and was extended to temperatures above > 400 °C which is undesirable. Contrary to those, 1.8 wt % Pd/FER material, after hydrothermal aging at 800 °C in 10 % H_2O vapor, showed no signs of deterioration [Figures 3, and S15]. This suggests that Pd ions indeed remain stabilized in their framework positions and are not accessible for water to hydrolyze them. Even after 850 °C HTA for 16 hours 50 % of the original NOx capacity remained [Figure S10].

We suggested earlier in this study that the reason for the shifting NOx release profile to lower temperatures resulted from the exothermicity of CO oxidation. In the presence of elevated CO levels (> 1000 ppm), CO oxidation may produce enough heat to create local over-heating and, consequently, release NOx at lower temperatures. We, therefore, performed PNA cycles on hydrothermally aged Pd/FER materials similar to those discussed in Figure 1 B. However, in this case we heated the sample only to 420 °C in each cycle (instead of the common 500 °C) simulating transient FTP (Figure 4 A) before returning to the initial adsorption temperature.

As the results in Figure 4 demonstrate, the quantity of adsorbed/released NO slightly changes after each cycle. The most striking feature, however, is the continuous shift in the initial NOx release temperature to lower values after each cycle. Figure 4 also exhibits the concentration profiles of CO during the consecutive NOx uptake/release cycles. Strikingly, the shift of the NOx release profile to lower temperatures perfectly follows the downward shift in the onset temperature of CO oxidation. These results directly prove that the initial sharp NOx release is coupled to CO oxidation in these materials. During CO oxidation, even at concentrations as low as ≈1000 ppm, local heating drives NOx off the adsorption sites. Simultaneously, a small number of isolated Pd sites gets reduced. This is the first observation of such local overheating caused by the heat of a reaction (here CO oxidation) benefiting the desorption profile of PNA materials and has important implications for regular vehicle catalyst testing protocols. In various studies,[30] high amounts of CO (up to a percent) are added to hydrocarbon oxidation streams and the performance of the catalysts is evaluated in the presence of such high CO amounts. Nano-"hot spots" from the local heat of CO oxidation (such hot spots are not easily picked-up by thermocouples) may affect the hydrocarbon oxidation profile and shift the conversion to lower temperatures, obscuring the real activity of the material (they would also affect water desorption, etc). In order to avoid potential ambiguity, evaluation of these oxidation catalysts should be performed both in the presence and absence of CO (or lower levels of CO) in the gas stream. Moreover, even for CO oxidation activity tests that utilize high amounts of CO, the light-off curves may not represent the intrinsic activity of the materials, and better (or worse) performance may be caused by nano-scale "hot spots" at flow rates relevant to vehicle exhaust. It is important to note that CO conversion profiles for this Pd/FER material allows for 90 % conversion of CO at

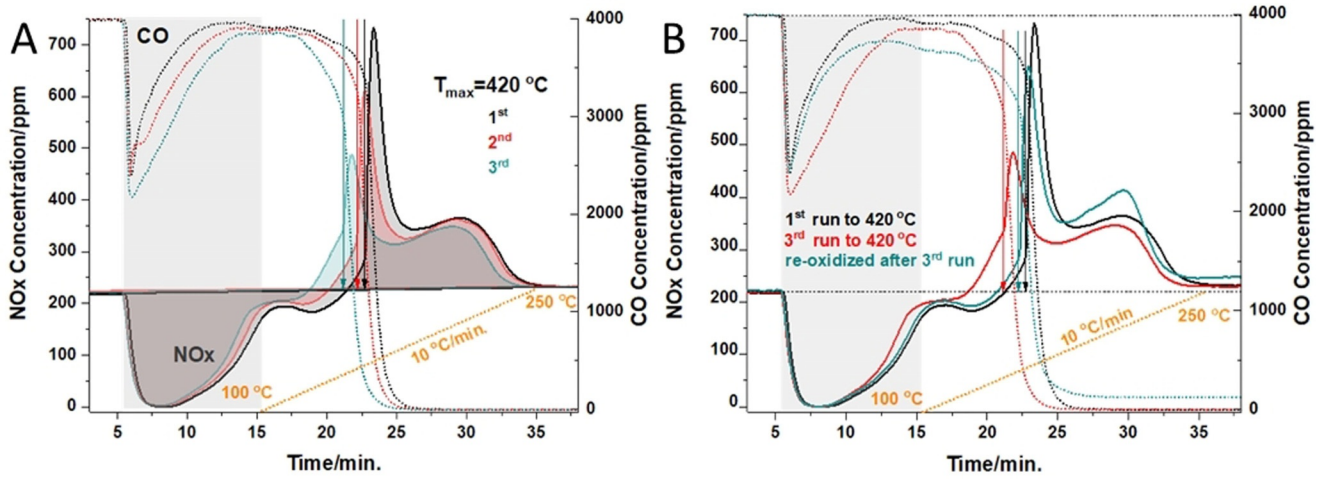

Figure 4. A. PNA performance for three consecutive cycles for 1.8 wt% Pd/FER (HTA). The maximum temperature terminating each cycle is restricted to 420 °C before cooling to 100 °C and initiating the subsequent PNA measurements. B. Comparison of PNA performance in the 1st and 3rd cycles with a maximum temperature of 420 °C, and for the sample reoxidized after the 3rd cycle in the presence of air at 700 °C.

temperatures ≈175–200 °C under practically relevant GHSV and gas mixtures. The increase in CO oxidation activity accompanied by a slight decrease in the NOx storage capacity in repeated cycles can be explained by changes to the speciation of Pd. Nanoscale "hot spots" not only lead to lower-temperature release of NOx from Pd sites but the temperatures achieved drive the Pd reduction and agglomeration (especially in the presence of CO and H_2O).[12] Since it is well known that Pd/PdO nanoparticles are much more active for CO oxidation than isolated Pd ions (especially on non-reducible supports),[28] the reduction of small amounts of Pd lead to removal of ionically dispersed Pd (*active for PNA*) and formation of nanoparticles (*active for CO oxidation*). However, the performance of PNA materials can be restored by heating to higher temperatures (≈650–700 °C, typically achieved by periodic regeneration of DPF or re-activation of SCR) that results in redispersion of the PdOx/Pd nanoparticles (Figure 4B). (We have also conducted long-term cyclic PNA experiments on the 1.8 wt% Pd/FER material. We found that the NOx storage capacity of this materials decreased by about 30% after 30 consecutive NOx uptake/release cycles (Figure S16). However, the initial performance could readily be restored by a brief ≈10 min calcination at 650–700 °C).

Conclusion

In summary, we have revealed the complex chemistry that occurs during PNA on single-atom Pd zeolite (SSZ-13 and FER) catalysts under practically relevant exhaust gas feeds. We provide deeper insight into the mechanisms of PNA storage, stability, and deactivation of Pd/zeolite materials as well as CO oxidation behavior during cold start. Notably, we found that thermal migration of Pd ions into specific positions in FER micropores produces a Pd^{II}/2Al that is resistant to hydrothermal aging up to 800 °C in the presence of 10% H_2O. At temperatures relevant to cold-start in the presence of CO in the gas feed, CO facilitates Pd to become accessible to NOx and enables NOx storage on such Pd^{II} atoms. We prepared a highly (hydro)thermally stable and active ≈1.9 wt% Pd/FER material in which the majority of expensive Pd is atomically dispersed and available to NOx storage, and which shows excellent performance under repeated cycling.

Acknowledgements

The research at PNNL was supported by the U.S. Department of Energy, Energy Efficiency and Renewable Energy, Vehicle Technology Office. Experiments were conducted in the Environmental Molecular Sciences Laboratory (EMSL), a national scientific user facility sponsored by the Department of Energy's Office of Biological and Environmental Research at Pacific Northwest National Laboratory (PNNL). PNNL is a multi-program national laboratory operated for the DOE by Battelle Memorial Institute under Contract DE-AC06-76RL01830. We acknowledge the support of CLEERS (Crosscut Lean Exhaust Emissions Reduction Simulations). CLEERS is an initiative funded by the U.S. Department of Energy (DOE) Vehicle Technologies Office to support the development of accurate tools for use in the design, calibration, and control of next generation engine/emissions control systems that maximize efficiency while complying with emissions regulations.

Conflict of Interest

The authors declare no conflict of interest.

Keywords: adsorption · NOx adsorbers · NOx uptake/release cycling · palladium · zeolites

[1] A. Wang, L. Olsson, *Nat. Catal.* **2019**, *2*, 566–570.

[2] T. Seiyama, T. Arakawa, T. Matsuda, N. Yamazoe, Y. Takita, *Chem. Lett.* **1975**, *4*, 781 – 784.
[3] S. I. Zones, US Patent 4 544 538, **1985**.
[4] J.-H. Kwak, R. G. Tonkyn, D. H. Kim, J. Szanyi, C. H. F. Peden, *J. Catal.* **2010**, *275*, 187 – 190.
[5] I. Bull, A. Moini, G. Koermer, J. Patchett, W. Jaglowski, S. Roth, US Patent US20070134146A1, **2010**.
[6] H.-Y. Chen, J. E. Collier, D. Liu, L. Mantarosie, D. Durán-Martín, V. Novák, R. Rajaram, D. Thompsett, *Catal. Lett.* **2016**, *146*, 1706 – 1711.
[7] K. Khivantsev, N. R. Jaegers, L. Kovarik, J. C. Hanson, F. F. Tao, Y. Tang, X. Zhang, I. Z. Koleva, H. A. Aleksandrov, G. N. Vayssilov, Y. Wang, F. Gao, J. Szanyi, *Angew. Chem. Int. Ed.* **2018**, *57*, 16672 – 16677; *Angew. Chem.* **2018**, *130*, 16914 – 16919.
[8] K. Khivantsev, N. R. Jaegers, L. Kovarik, S. Prodinger, M. A. Derewinski, Y. Wang, F. Gao, J. Szanyi, *Appl. Catal. A* **2019**, *569*, 141 – 148.
[9] K. Khivantsev, N. R. Jaegers, I. Z. Koleva, H. A. Aleksandrov, L. Kovarik, M. Engelhard, F. Gao, Y. Wang, G. N. Vayssilov, J. Szanyi, *J. Phys. Chem. C* **2020**, *124*, 309 – 321.
[10] K. Khivantsev, F. Gao, L. Kovarik, Y. Wang, J. Szanyi, *J. Phys. Chem. C* **2018**, *122*, 10820 – 10827.
[11] M. Moliner, A. Corma, *React. Chem. Eng.* **2019**, *4*, 223 – 234.
[12] K. Khivantsev, N. R. Jaegers, L. Kovarik, J. Z. Hu, F. Gao, Y. Wang, J. Szanyi, *Emiss. Control Sci. Technol.* **2020**, *6*, 126 – 138.
[13] E. Bello, V. J. Margarit, E. M. Gallego, F. Schuetze, C. Hengst, A. Corma, M. Moliner, *Microporous Mesoporous Mater.* **2020**, *302*, 110222.
[14] K. Khivantsev, N. Jaegers, L. Kovarik, M. Wang, J. Z. Hu, M. Derewinski, J. Szanyi, *Appl. Catal. B* **2021**, *280*, 119449.
[15] R. R. Rajaram, H.-Y. Chen, D. Liu, US Patent US20150158019A1, **2015**.
[16] Y. Ji, S. Bai, M. Crocker, *Appl. Catal. B* **2015**, *170 – 171*, 283 – 292.
[17] O. Mihai, L. Trandafilović, T. Wentworth, F. F. Torres, L. Olsson, *Top. Catal.* **2018**, *61*, 2007 – 2020.
[18] R. Jonsson, J. Woo, M. Skoglund, L. Olsson, *Catalysts* **2020**, *10*, 173 – 189.
[19] Y. Ji, D. Xu, S. Bai, U. Graham, M. Crocker, B. Chen, C. Shi, D. Harris, D. Scapens, J. Darab, *J. Ind. Eng. Chem. Res.* **2017**, *56*, 111 – 125.
[20] K. Khivantsev, J. Szanyi, N. R. Jaegers, L. Kovarik, F. Gao, Y. Wang, US Patent US11071966B2, **2021**.
[21] L. Castoldi, R. Matarrese, S. Morandi, P. Ticali, L. Lietti, *Catal. Today* **2021**, *360*, 317 – 325.
[22] A. Porta, T. Pellegrinelli, L. Castoldi, R. Matarrese, S. Morandi, S. Dzwigaj, L. Lietti, *Top. Catal.* **2018**, *61*, 2021 – 2034.
[23] Y. Ji, S. Bai, D. Xu, D. Qian, Z. Wu, Y. Song, R. Pace, M. Crocker, K. Wilson, A. Lee, D. Harris, D. Scapens, *Appl. Catal. B* **2020**, *264*, 118499.
[24] Y. S. Ryou, J. Lee, S. Cho, H. Lee, C. H. Kim, D. H. Kim, *Appl. Catal. B* **2017**, *212*, 140 – 149.
[25] Y. S. Ryou, J. Lee, H. Lee, C. H. Kim, D. H. Kim, *Catal. Today* **2019**, *320*, 175 – 180.
[26] J. Lee, Y. Ryou, S. Hwang, Y. Kim, S. Cho, H. Lee, C. H. Kim, D. H. Kim, *Catal. Sci. Technol.* **2019**, *9*, 163 – 173.
[27] Y. Kim, S. Hwang, J. Lee, Y. S. Ryou, H. Lee, C. H. Kim, D. H. Kim, *Emiss. Control Sci. Technol.* **2019**, *5*, 172 – 182.
[28] X. I. Pereira-Hernandez, A. DelaRiva, D. Kunwar, H. Xiong, B. Sudduth, M. Engelhard, L. Kovarik, V. Muravev, E. J. Hensen, Y. Wang, A. K. Datye, *Nat. Commun.* **2019**, *10*, 1358.
[29] M. C. Dalconi, A. Alberti, G. Cruciani, *J. Phys. Chem. B* **2003**, *107*, 12973 – 12980.
[30] K. G. Rappé, et al., *Emiss. Control Sci. Technol.* **2019**, *6*, 1 – 32.

Manuscript received: June 6, 2021
Accepted manuscript online: October 7, 2021
Version of record online: December 3, 2021